



The nature of the copper sulfide film grown on copper in aqueous sulfide and chloride solutions

Mengnan Guo¹ | Jian Chen¹  | Taylor Martino¹ | Christina Lilja² | Johannes A. Johansson² | Mehran Behazin³ | Wilfred J. Binns³ | Peter G. Keech³ | James J. Noël^{1,4}  | David W. Shoesmith^{1,4}

¹Department of Chemistry, University of Western Ontario, London, Ontario, Canada

²Swedish Nuclear Fuel and Waste Management Co., Solna, Sweden

³Nuclear Waste Management Organization, Toronto, Ontario, Canada

⁴Surface Science Western, London, Ontario, Canada

Correspondence

Jian Chen and James J. Noël, Department of Chemistry, University of Western Ontario, London, ON N6A 5B7, Canada. Email: jchen496@uwo.ca (J. C.) and jjnoel@uwo.ca (J. J. N.)

Funding information

Nuclear Waste Management Organization; Svensk Kärnbränslehantering AB

Abstract

In this paper, the properties of copper sulfide films formed both anodically and naturally in deaerated/anoxic aqueous sulfide and chloride solutions were investigated using a series of electrochemical and surface analytical techniques. A combination of cyclic voltammetric, corrosion potential (E_{corr}), and cathodic stripping voltammetric experiments showed that the sulfide film growth kinetics and film morphologies were controlled by the supply of SH^- from the bulk solution to the copper surface. There was no passive barrier layer observed on the copper surface under either electrochemical or corrosion conditions. The film morphology was dependent on the type and concentration of anions (SH^- , Cl^-) present in the solution. Scanning electron microscopy on both surfaces and focused ion beam-cut cross-sections showed the growth of a thin, but porous, base layer of chalcocite (Cu_2S) after short immersion periods (up to 2 hr) and the continuous growth of a much thicker crystalline outer deposit over longer immersion periods (≥ 36 hr), suggesting a solution species transport-based film formation process and the formation of an ineffective thin “barrier-type” layer on copper.

KEYWORDS

copper, corrosion, nuclear waste disposal, sulfide

1 | INTRODUCTION

The safe disposal and management of high-level nuclear waste (HLNW) is a concern for many countries, such as Sweden, Finland, and Canada, which rely heavily on nuclear power to generate electricity. The universally chosen approach for the permanent disposal of the HLNW is to bury it at a depth of ≥ 500 m in a deep geological repository (DGR) with multiple barriers to provide safe containment and isolation.^[1,2] A primary barrier in this multibarrier system is a corrosion-resistant container capable of withstanding the anticipated hydrostatic, lithostatic, and glacial loads.^[1] The

proposed container in some countries will be designed with either a cylindrical copper (Cu) shell containing a nodular cast iron insert (Sweden, Finland) or a Cu-coated carbon steel vessel (Canada).

Upon emplacement, this container will initially be exposed to humid, warm, and slightly oxidizing conditions, which will then rapidly evolve to hot and dry, before gradually becoming cool and anoxic as γ -radiation fields emitted by the wasteform inside the container decay. Entrapped O_2 , trapped in the DGR upon sealing, will be consumed by mineral and microbial reactions occurring in the bentonite clay compacted around the container and

the corrosion of structural steel within the repository, as well as slight corrosion of the container copper itself.^[2] Owing to the extremely small inventory of these oxidizing species, waste containers can be readily designed to survive the early oxidizing period. However, the long-term threat to container durability is the presence of sulfide (SH^-) within the groundwater, as this species can cause degradation of the copper.

As illustrated in Figure 1, sulfide can be produced by the dissolution of minerals and/or the microbial activity of sulfate-reducing bacteria in the clay at locations remote from the container surface. This process is expected to have a very small impact on the bulk concentration of sulfide within the groundwater, raising it to perhaps <0.1 ppm; however,^[3,4] the subsequent transport of sulfide to the container surface will lead to its corrosion, involving the formation of a chalcocite (Cu_2S) surface film or a more porous deposit. Considerable effort has been expended on the investigation of the copper sulfide film formation process.^[5–15] The physical properties of this chalcocite film have been demonstrated to vary significantly with sulfide concentration $[\text{SH}^-]$, the flux of SH^- to the Cu surface, and the presence of other groundwater anions (such as Cl^- and SO_4^{2-}). The morphology of the surface film will influence the manner in which the corrosion will progress on the Cu surface. If a passive film is formed, Cu could be susceptible to pitting, with corrosion damage occurring preferentially at localized sites. By contrast, if the deposit is not protective, then the corrosion damage would be more uniformly distributed.

In this study, we have investigated the formation of Cu_2S films grown under both electrochemical and natural corrosion conditions using a combination of electrochemical and surface analytical techniques. Our primary goal was to investigate the early stages of sulfide film growth to determine whether there was any evidence for the formation of a barrier layer that could support pitting. Scanning electron microscopy (SEM) and energy-dispersive X-ray spectroscopy

(EDX) were performed on both electrochemically and corroded Cu surfaces. Focused ion beam (FIB) cross-sectioning coupled with SEM was also used to examine the damage incurred at the Cu surface.

2 | EXPERIMENTAL

2.1 | Sample preparation

The Cu used in all experiments was P-doped (30–100 wt ppm) O-free copper (<5 wt ppm) provided by the Swedish Nuclear Fuel and Waste Management Co. (SKB).^[16] Cu disk working electrodes with a total surface area of 0.785 cm^2 were cut from the plate material. The disks were connected to a stainless-steel shaft and painted with a nonconductive lacquer to prevent contact of the steel with the electrolyte. The electrodes were then heated (60°C for 12 hr) to promote the adhesion of the paint. The exposed flat surface was ground successively with 240, 600, 800, 1,000, and 1,200 grade SiC paper, and then it was polished to a mirror finish using 1-, 0.3-, and $0.05\text{-}\mu\text{m}$ Al_2O_3 suspensions. Before experiments, electrodes were washed with Type I water (resistivity = $18.2\text{ M}\Omega\text{-cm}$, obtained from a Thermo Scientific Barnstead Nanopure 7143 Ultrapure Water System), ultrasonically cleaned using methanol (reagent grade), washed with Type I water, and then dried using a stream of ultrapure Ar (99.999%).

2.2 | Electrochemical/corrosion cell and instrumentation

A three-electrode glass electrochemical cell was used in the electrochemical and corrosion experiments with a platinum plate (99.95%; Alfa Aesar) connected to external circuitry by a Pt wire (0.5-mm diameter) as the counter electrode, a

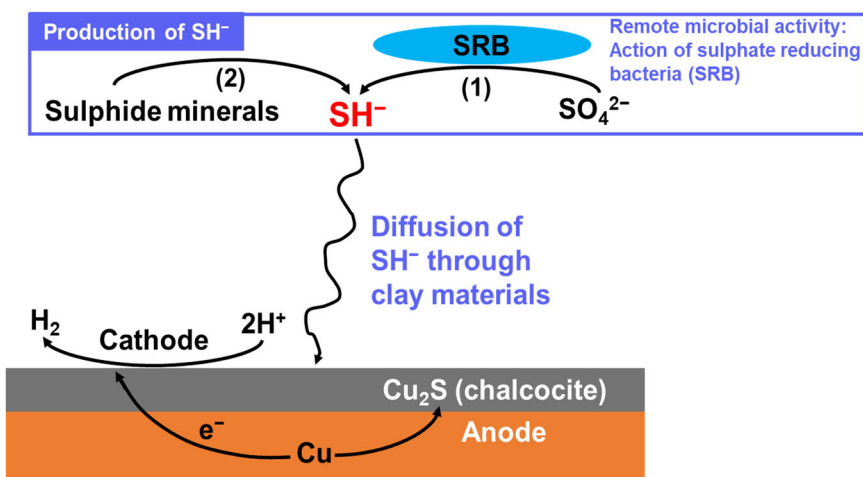


FIGURE 1 A schematic diagram showing that the long-term corrosion process that could lead to container failure is the remote production of sulfide by the action of sulfate-reducing bacteria [Color figure can be viewed at wileyonlinelibrary.com]

saturated calomel reference electrode (SCE; 0.242 V/SHE), and a Cu working electrode. The cell was housed inside a Faraday cage to reduce electrical noise from external sources. All electrochemical experiments were conducted using either a Cu stationary electrode or a rotating disk electrode (RDE), as indicated in Figure 2. The electrode rotation rate was controlled by a Pine Instrument Company Analytical Rotator Model AFA86 Serial 882, and electrochemical measurements were made using a 1287 Solartron potentiostat or a Solartron Analytical ModuLab equipped with CorrWare (Scribner Associates, Version 3.5h) and XM-Studio-ECS software (Version 3.4).

Corrosion experiments were performed in an Ar-purged anaerobic chamber (Canadian Vacuum Systems Ltd.), maintained at a positive pressure (2–4 mbar) by an MBraun glove box control system. The oxygen concentration in the chamber was analyzed with an MBraun oxygen probe with a detection limit of 1 ppm. The chamber was maintained at a total oxygen concentration ≤ 3 ppm, with the dissolved oxygen in solution calculated, using Henry's law, to be $\leq 3.9 \times 10^{-9}$ M. Despite the possible presence of trace amounts of dissolved oxygen in the sulfide solution, the oxidation of Cu to copper sulfide would still be the predominant process, as copper sulfide is more stable in a sulfide solution than copper oxide, based on thermodynamic data ($\Delta G^\circ = -101.46$ kJ/mol for the conversion from Cu_2O to Cu_2S in sulfide solutions at 298 K^[7]: $\text{Cu}_2\text{O}(\text{s}) + \text{SH}^-(\text{aq}) \rightarrow \text{Cu}_2\text{S}(\text{s}) + \text{OH}^-(\text{aq})$) and available literature.^[17–19]

2.3 | Electrolyte preparation

Solutions were prepared with reagent-grade sodium chloride (NaCl; 99.0% assay; Thermo Fisher Scientific),

sodium sulfide ($\text{Na}_2\text{S} \cdot 9\text{H}_2\text{O}$; 98.0% assay; Sigma-Aldrich), boric acid (H_3BO_3 ; 99.5% assay; Caledon), sodium borate decahydrate ($\text{Na}_2\text{B}_4\text{O}_7 \cdot 10\text{H}_2\text{O}$; 99.5% assay; Sigma-Aldrich), sodium sulfate (Na_2SO_4 ; 101.5% assay; Sigma-Aldrich), and Type I water (18.2 M Ω ·cm). The sulfide concentrations were significantly higher than those expected within a DGR.^[2,20–22] The predicted sulfide concentration ranges from 1.2×10^{-7} to 1.2×10^{-4} M with the peaksulfide flux to the container surface is $< 10^{-10}$ mol/(m²·s) in a final repository at the Forsmark site.^[21] Experiments were conducted in solutions containing low $[\text{SH}^-]$ and medium $[\text{Cl}^-]$ (5×10^{-5} M $\text{Na}_2\text{S} + 1$ M NaCl), high $[\text{SH}^-]$ and high $[\text{Cl}^-]$ (5×10^{-4} M $\text{Na}_2\text{S} + 3$ M NaCl), and medium $[\text{SH}^-]$ and low $[\text{Cl}^-]$ (2×10^{-4} M $\text{Na}_2\text{S} + 0.1$ M NaCl). To ensure the maintenance of a deaerated environment and to minimize sulfide oxidation for benchtop experiments, the solutions were sparged with Ar for ≥ 30 min before each experiment and purged continuously throughout the experiment.

2.4 | Electrochemical experiments

Cyclic voltammetric (CV) studies were performed using an RDE. Before applying a voltammetric scan, the electrode was cathodically cleaned at -1.5 V/SCE for 60 s to reduce air-formed oxides and then at -1.15 V/SCE for another 60 s to allow the detachment of H_2 bubbles that may have formed at the more negative potential (-1.5 V/SCE). Voltammetric scans were performed from an initial potential, ranging from -1.5 V/SCE to -1.35 V/SCE, to a final potential, ranging between -0.7 V/SCE and -0.5 V/SCE, at a scan rate of either 2 mV/s or 10 mV/min. The choice of starting potential

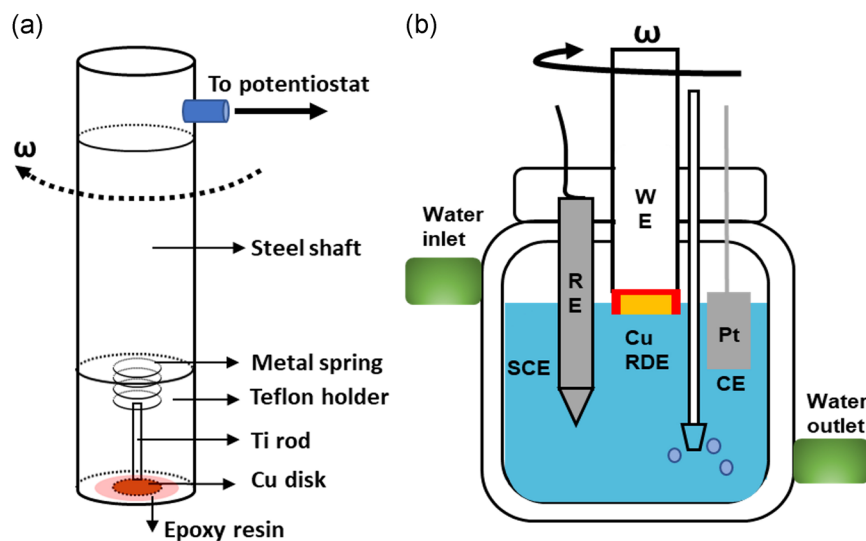


FIGURE 2 A schematic showing (a) a Cu rotating disk electrode (RDE) and (b) an electrochemical cell with an RDE working electrode [Color figure can be viewed at wileyonlinelibrary.com]

had no influence on the subsequent electrochemical behavior. All experiments were conducted at room temperature ($21 \pm 2^\circ\text{C}$).

2.5 | Corrosion experiments

After cathodic cleaning (Section 2.4), the Cu electrodes were immersed in the sulfide solution for various exposure periods. After short immersion periods (i.e., ≤ 36 hr), cathodic stripping voltammetric (CSV) scans were performed from the corrosion potential (E_{corr}) to -1.4 V/SCE at a scan rate of 10 mV/min to reduce the sulfide film. All experiments were performed at $21 \pm 2^\circ\text{C}$.

2.6 | Surface analyses

Before surface analysis, the corroded Cu electrodes were rinsed with Type I water, dried with a stream of ultrapure Ar gas, and stored in the anaerobic chamber. Analyses were then performed after a minimal period of interim storage. The surface and cross-sectional morphologies of corroded specimens were examined using a Leo 1540 SEM equipped with a FIB (Zeiss Nano Technology Systems Division, Germany). The composition of films was qualitatively analyzed by EDX using a Leo 1540 FIB/SEM (the oxygen detection limit is 1 at%).

3 | RESULTS AND DISCUSSION

3.1 | Films grown anodically under controlled convective conditions

Figure 3 shows films formed anodically and reduced cathodically under controlled convective conditions using RDEs. At low $[\text{SH}^-]$ and medium $[\text{Cl}^-]$ (i.e., 5×10^{-5} M $\text{Na}_2\text{S} + 1.0$ M NaCl), the anodic current density on the reverse scan retraced the current density recorded on the forward scan, demonstrating that, as shown previously,^[8] the anodically formed Cu_2S film was porous and able to sustain growth when the potential was reduced. The signature for a passive film would have been a current density reduced to zero on the reverse scan, as the electric field within the film decreased below the value required to maintain its growth. The single cathodic reduction peak observed on the reverse scan indicated the formation of a single-layered film. The amount of Cu_2S formed, expressed as a charge (Q), was obtained by calculating the area associated with the cathodic reduction peak, as indicated by the shaded area in region Q_B (Figure 3a). As observed previously, the amount of

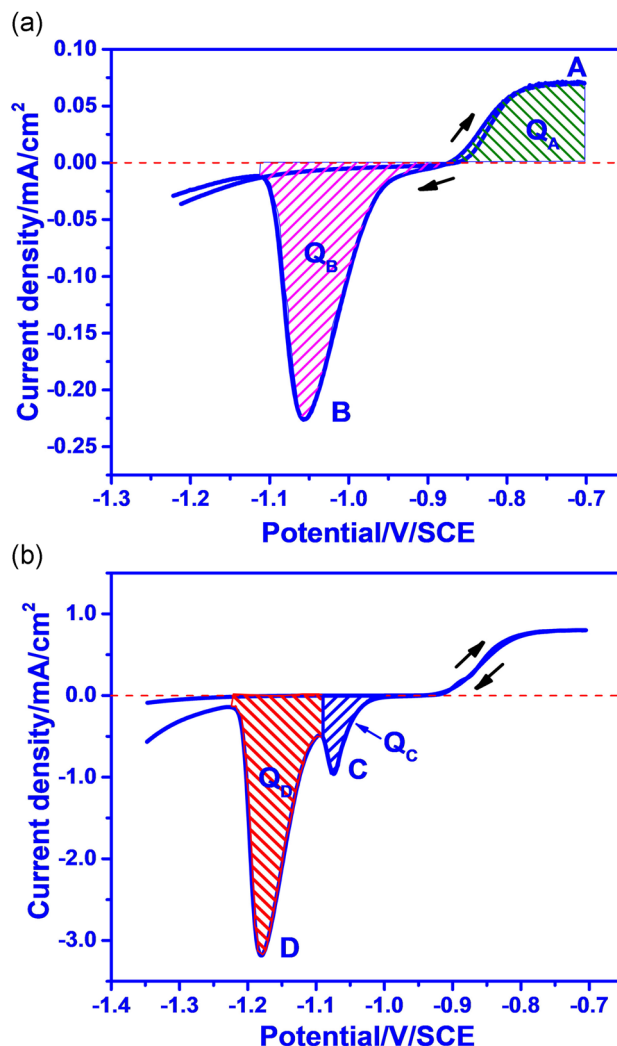


FIGURE 3 Cyclic voltammetric (CV) recorded at an electrode rotation rate of 25 Hz in deaerated solutions containing various concentrations of sulfide and chloride: (a) CV recorded at low $[\text{SH}^-]$ and medium $[\text{Cl}^-]$ (5×10^{-5} M $\text{Na}_2\text{S} + 1.0$ M NaCl), (b) CV recorded at high $[\text{SH}^-]$ and high $[\text{Cl}^-]$ (5×10^{-4} M $\text{Na}_2\text{S} + 3.0$ M NaCl) [Color figure can be viewed at wileyonlinelibrary.com]

charge associated with the anodic film formation (region A [$2Q_A$] in Figure 3a) was approximately equal to the amount of charge recovered by the cathodic reduction in region B (Q_B), confirming that all anodically formed Cu_2S films on the forward scan were completely reduced on the reverse scan. When the $[\text{SH}^-]$ and $[\text{Cl}^-]$ were high (i.e., 5×10^{-4} M $\text{Na}_2\text{S} + 3.0$ M NaCl), Figure 3b, the anodic current–potential profile was similar to that observed at low $[\text{SH}^-]$ and medium $[\text{Cl}^-]$; however, the value of the plateau current density was lower. This decrease in plateau current density has been shown to be due to a competition between SH^- and Cl^- for adsorption sites on the Cu surface.^[11] Although $[\text{SH}^-]$ had been increased by an order of magnitude, the anodic current density

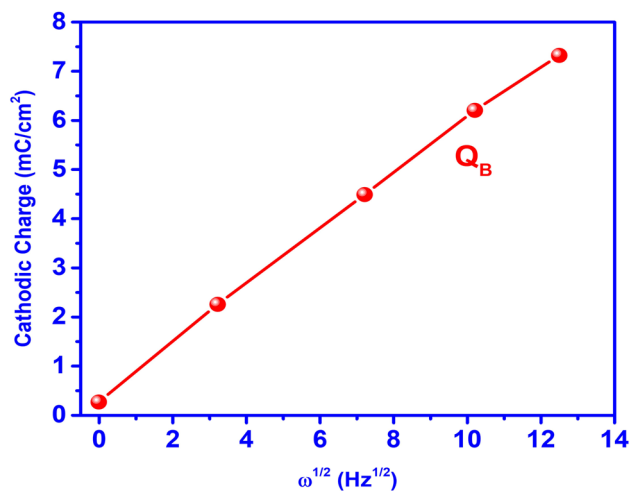


FIGURE 4 Cathodic charge (Q_B) plotted as a function of the electrode rotation rate (ω) calculated from cyclic voltammetric recorded in solutions containing 5×10^{-5} M Na_2S + 1.0 M NaCl [Color figure can be viewed at wileyonlinelibrary.com]

remained the same on the reverse scan as it was on the forward scan, consistent with the presence of a porous film.^[8] However, two cathodic reduction peaks were observed (regions C and D), suggesting the presence of either two distinct morphological forms of the same phase or, possibly, two different copper sulfide phases. Previous XRD results demonstrated that only chalcocite (Cu_2S) was present,^[5] which points to two different morphological forms of the same phase, for example, two different layers.

The extent of Cu_2S film growth for films grown at low $[\text{SH}^-]$ and medium $[\text{Cl}^-]$ (expressed as an electrochemical charge [Q_B]), determined from CVs as described above, increased with an increase in electrode rotation rate (Figure 4). This demonstrated that the rate, and hence the extent, of the film growth was dominantly determined by the flux of SH^- to the copper surface. More comprehensive studies have shown that film growth is partially controlled by the SH^- flux and partially by the interfacial kinetics.^[9,11]

Figure 5 shows the charges associated with the reduction peaks C and D, recorded as a function of the electrode rotation rate, in solutions containing a high $[\text{SH}^-]$ and high $[\text{Cl}^-]$. Under stagnant conditions, the cathodic charge associated with peak D (Q_D) was negligible, suggesting that only film C was formed when the flux of SH^- to the Cu surface was low. At the higher fluxes of SH^- achieved at higher electrode rotation rates, peak C achieved an approximately constant cathodic charge (Q_C), whereas the charge associated with peak D (Q_D) continually increased. This indicated the establishment of a constant film thickness associated with the film

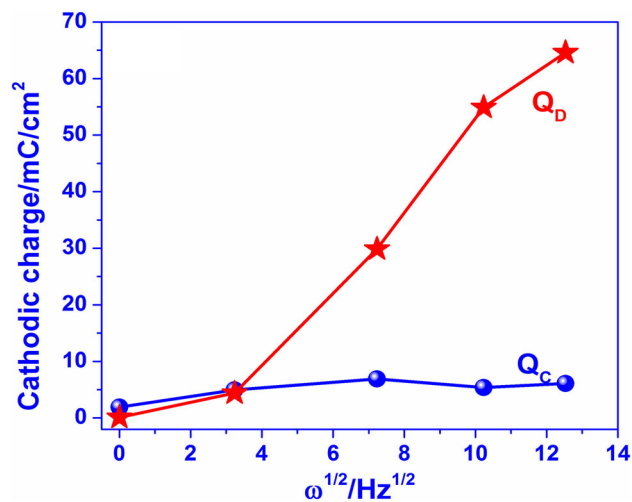


FIGURE 5 Cathodic charges (Q_C and Q_D) plotted as a function of the electrode rotation rate (ω) calculated from cyclic voltammetric recorded in solutions containing 5×10^{-4} M Na_2S + 3.0 M NaCl [Color figure can be viewed at wileyonlinelibrary.com]

reduced at peak C, but a flux-dependent growth of the film reduced at peak D. This observation was consistent with the rapid growth of a porous base layer to a limited thickness, accompanied by the growth of a much thicker outer layer.

3.2 | Films grown under freely corroding conditions

Cu electrodes were immersed in a solution containing 0.2-M borate (pH 9), 2×10^{-4} M Na_2S , and 0.1-M $[\text{Cl}^-]$ for various immersion times, ranging from 0.5 to 36 hr. The presence of borate in these experiments served two purposes: (a) it buffered the pH and (b) it reproduced the conditions used by others who have claimed that the copper sulfide layer formed was passive.^[20,21] As noted above, selected sulfide concentrations were significantly higher than those generally anticipated in an actual DGR.^[2,22–24] The E_{corr} was monitored continuously, and it rapidly attained a steady-state value within the range of approximately -850 ± 20 mV/SCE (Figure 6). This value was close to the equilibrium potential for Cu/ Cu_2S at this $[\text{SH}^-]$ (-1.0 V/SCE), which was an observation consistent with the rapid growth of Cu_2S requiring only a small anodic overpotential.

Figure 7a shows a series of CSVs recorded after the various durations of corrosion. Depending on the duration of the corrosion experiment, one or two cathodic reduction peaks (E and F) are observed in the CSVs. The charge associated with peak E and the total charge for both peaks E and F as a function of the period of

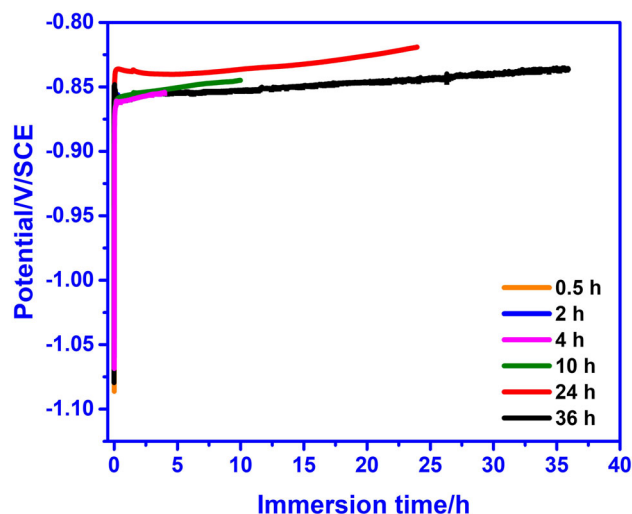


FIGURE 6 Corrosion potentials measured on Cu for various durations of immersion in deaerated solutions containing 2×10^{-4} M Na_2S + 0.1 M NaCl solution buffered with 0.2-M borate (pH 9). SCE, saturated calomel reference electrode [Color figure can be viewed at wileyonlinelibrary.com]

corrosion are shown in Figure 7b. Attempts to calculate Q_F were complicated by water reduction at potentials below -1.1 V/SCE; thus, results were only semi-quantitative when the exposure period exceeded 10 hr. Despite this uncertainty, the values in Figure 7b clearly demonstrated that the film reduced at peak E rapidly grew to a constant thickness, regardless of the exposure period, whereas the film reduced at peak F continued to grow over longer exposure periods. It is interesting to compare these results from varying exposure times of the freely corroding system to those in Section 3.1 where similar electrochemical reduction features were observed as peaks C and D. Specifically, Q_E was insensitive to the increased rotation rate (sulfide flux; Figure 5) and exposure time (Figure 7b), whereas Q_F increased as a function of both. These results are consistent with the rapid growth of a thin surface layer (i.e., the feature reduced at peak E), which rapidly became sufficiently porous to allow the continuous development of a second outer deposit reduced at peak F. One reasonable explanation for this was the rapid growth of a thin base layer, which may have initially been coherent; however, it rapidly developed porosity to relieve the large interfacial stress that developed due to the large Pilling–Bedworth ratio ($\mathcal{R}_{\text{PB}} = 2$) of Cu_2S .^[25]

Figure 8 shows the surface morphologies and cross-sections of two corroded Cu samples after immersion for 2 and 36 hr, respectively, in borate-buffered (pH 9) solutions containing 2×10^{-4} M Na_2S + 0.1 M NaCl. After 2 hr of immersion, the Cu surface was covered with a uniform particulate deposit, Figure 8a, whereas after a similar 2 hr of

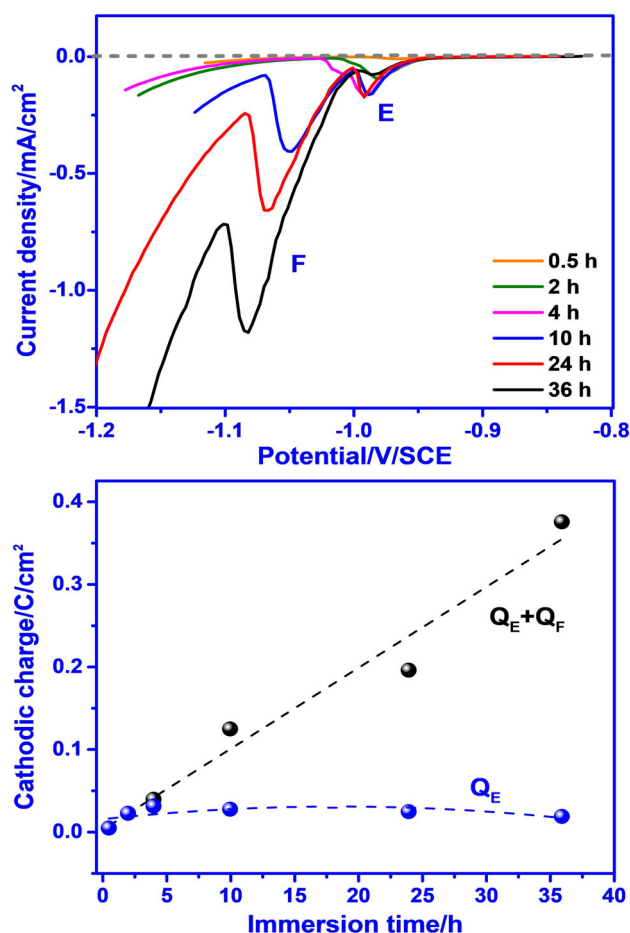


FIGURE 7 (a) Cathodic stripping voltammograms recorded after various periods of immersion in deaerated 2×10^{-4} M Na_2S + 0.1 M NaCl solution buffered with 0.2-M borate (pH 9), (b) cathodic charges, Q_E and Q_F , plotted as a function of immersion time. SCE, saturated calomel reference electrode [Color figure can be viewed at wileyonlinelibrary.com]

exposure, the CSVs in Figure 7a showed only peak E. The FIB-cut cross-section of the 2-hr exposure specimen, Figure 8b, confirmed that this layer was distributed uniformly across the surface at a thickness below 100 nm, but it was also porous. Besides having obvious porosity, the film was both too thick and too irregular in topography to be a coherent passive film formed by point defect transport processes.^[20,21] On the basis of the cathodic charges obtained from the CSVs and the theoretical density of chalcocite,^[26] the average film thickness of this base layer, if uniformly distributed across the surface, should have been in the range 25–45 nm.

After 36 hr of corrosion, the surface was covered with a much thicker crystalline deposit, as shown in the top-down and FIB-cut cross-section SEM images, Figures 8c and 8d, respectively, with crystals at some locations achieving heights of ~ 1 μm . Although the location of the previously discussed base layer and its apparent thickness

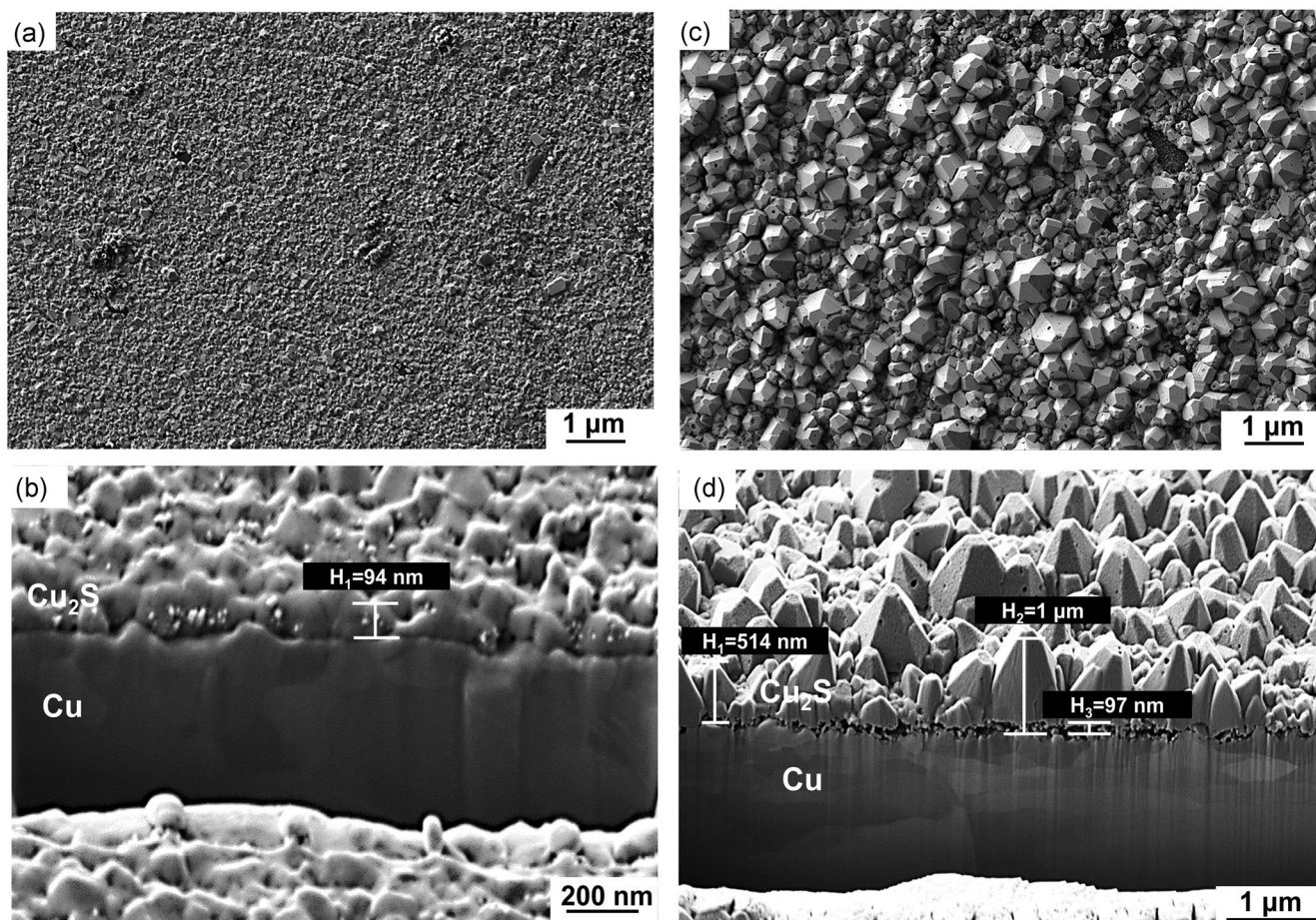


FIGURE 8 Scanning electron microscopy (SEM) and focused ion beam (FIB)-cut cross-sectional images of films grown in a borate-buffered (pH 9) solution containing 2×10^{-4} M Na_2S + 0.1 M NaCl . (a and b) SEM micrographs of the surfaces of the film as grown and FIB-cut cross-section after 2-hr immersion. (c and d) SEM micrographs of the surfaces of the film as grown and FIB-cut cross-section after 36-hr immersion

are indicated in Figure 8d, they are difficult to observe, owing to the presence of much larger features. The formation of such a thick crystalline outer deposit was consistent with our previous observations^[6–15] and with our demonstration that growth of this deposit occurred at the film/solution interface, supported by the transport through the pores of the base layer of Cu(I), as both sulfide complexes ($\text{Cu}(\text{SH})_2^-$) and Cu_3S_3 clusters, formed at the Cu surface.^[15,24–29]

4 | CONCLUSIONS

Electrochemical and corrosion studies showed that, depending on the sulfide and chloride concentrations, the chalcocite (Cu_2S) film grown on Cu was composed of one or two layers: a thin base layer and an outer deposited thicker layer. At low concentrations, only one layer was formed, and the formation of the dual layer was observed with the increase in the concentration.

Although the base layer might have been a barrier layer initially, it rapidly became porous and stopped growing. This layer developed a topography inconsistent with a passive barrier layer grown by the transport of point defects through the growing film.

Subsequently, an outer layer deposited and continued to grow at a rate partially controlled by the flux of sulfide to the copper surface. The crystalline nature of this outer deposited layer was consistent with previous claims that the layer grew by the transport of Cu (I) species, as complexes and clusters, through the porous base layer.

ACKNOWLEDGMENTS

The authors would like to thank Fraser King (Integrity Corrosion Consulting; Nanaimo, BC, Canada) for many helpful discussions and suggestions, and Western Nanofabrication Facility for assisting in SEM/FIB analyses. This study was funded by the Swedish Nuclear Fuel and Waste Management Company (SKB; Solna, Sweden),

Posiva Oy (Olkiluoto, Finland), and the Nuclear Waste Management Organization (Toronto, Canada).

ORCID

Jian Chen  <http://orcid.org/0000-0003-4021-7127>

James J. Noël  <http://orcid.org/0000-0003-3467-4778>

REFERENCES

- [1] T. Standish, J. Chen, R. Jacklin, P. Jakupi, S. Ramamurthy, D. Zagidulin, P. Keech, D. Shoesmith, *Electrochim. Acta* **2016**, *211*, 331.
- [2] F. King, D. S. Hall, P. G. Keech, *Corros. Eng., Sci. Technol.* **2017**, *52*, 25.
- [3] Nuclear Waste Management Organization Technical Report, NWMO TR-2017-02, **2017**.
- [4] F. Garisto, Nuclear Waste Management Organization Technical Report, NWMO TR-2017-08, **2017**.
- [5] J. Chen, Z. Qin, D. W. Shoesmith, *J. Electrochem. Soc.* **2010**, *157*, C338.
- [6] J. Chen, Z. Qin, D. W. Shoesmith, *Electrochim. Acta* **2011**, *56*, 7854.
- [7] J. Chen, Z. Qin, L. Wu, J. J. Noël, D. W. Shoesmith, *Corros. Sci.* **2014**, *87*, 233.
- [8] T. Martino, R. Partovi-Nia, J. Chen, Z. Qin, D. W. Shoesmith, *Electrochim. Acta* **2014**, *127*, 439.
- [9] T. Martino, J. Chen, Z. Qin, D. W. Shoesmith, *Corros. Eng., Sci. Technol.* **2017**, *52*, 61.
- [10] T. Martino, J. Smith, J. Chen, Z. Qin, J. J. Noël, D. W. Shoesmith, *J. Electrochem. Soc.* **2019**, *166*, C9.
- [11] T. Martino, J. Chen, J. J. Noël, D. W. Shoesmith, *Electrochim. Acta* **2019**, 135319.
- [12] J. Chen, Z. Qin, D. W. Shoesmith, *Corros. Eng., Sci. Technol.* **2014**, *49*, 415.
- [13] J. Chen, Z. Qin, T. Martino, D. W. Shoesmith, *Corros. Eng., Sci. Technol.* **2017**, *52*, 40.
- [14] J. Chen, Z. Qin, T. Martino, M. Guo, D. W. Shoesmith, *Corros. Sci.* **2018**, *131*, 245.
- [15] J. Chen, Z. Qin, T. Martino, D. W. Shoesmith, *Corros. Sci.* **2017**, *114*, 72.
- [16] Svensk Kärnbränslehantering AB, Technical Report, TR-10-14, **2010**.
- [17] J. M. Smith, J. C. Wren, M. Odziemkowski, D. W. Shoesmith, *J. Electrochem. Soc.* **2007**, *154*, C431.
- [18] H. M. Hollmark, P. G. Keech, J. R. Vegelius, L. Werme, L.-C. Duda, *Corros. Sci.* **2012**, *54*, 85.
- [19] E. M. Khairy, N. A. Darwish, *Corros. Sci.* **1973**, *13*, 149.
- [20] A. Gordon, H. Pahverk, E. Börjesson, L. Sjögren, O. Karlsson, H. Bergqvist, F. Lindberg, A. Johansson, *Corrosion Morphology of Copper in Anoxic Sulphide Environments*, Svensk Kärnbränslehantering AB, Technical Report, TR-18-14, **2018**.
- [21] Supplementary Information on Canister Integrity Issues, Svensk Kärnbränslehantering AB, Technical Report, TR-19-15, **2019**.
- [22] D. S. Hall, P. G. Keech, *Corros. Eng., Sci. Technol.* **2017**, *52*, 2.
- [23] C. Dong, F. Mao, S. Gao, S. Sharifi-Asl, P. Lu, D. D. Macdonald, *J. Electrochem. Soc.* **2016**, *163*, C707.
- [24] T. L. Martino, *Ph.D. Thesis*, Western University (London, UK) **2018**.
- [25] M. Guo, J. Chen, T. Martino, M. Biesinger, J. J. Noël, D. W. Shoesmith, *J. Electrochem. Soc.* **2019**, *166*, C550.
- [26] F. King, J. Chen, Z. Qin, D. Shoesmith, C. Lilja, *Corros. Eng., Sci. Technol.* **2017**, *52*, 210.
- [27] D. A. Crerar, H. L. Barnes, *Econ. Geol.* **1976**, *71*, 772.
- [28] B. W. Mountain, T. M. Seward, *Geochim. Cosmochim. Acta* **1999**, *63*, 11.
- [29] G. W. Luther, S. M. Theberge, T. F. Rozan, D. Rickard, C. C. Rowlands, A. Oldroyd, *Environ. Sci. Technol.* **2002**, *36*, 394.

How to cite this article: Guo M, Chen J, Martino T, et al. The nature of the copper sulfide film grown on copper in aqueous sulfide and chloride solutions. *Materials and Corrosion*. 2021;72: 300–307. <https://doi.org/10.1002/maco.202011710>